

Dedicated to.....

My beloved parents

Declaration of Academic Integrity

"I declare that this written submission represents my ideas in my own words and where other's ideas or words have been included, I have adequately cited and referenced the original sources. I also declare that I have adhered to all principles of academic honesty and integrity and have not misrepresented or fabricated or falsified any idea/data/fact/source in my submission. I understand that any violation of the above will be cause for disciplinary action as per the rules and regulations of the Institute."

Date: 21-11-2023

Place: Tezpur University

Suman Lahkar
(Suman Lahkar)

Regn No. TZ156024 of 2015

All rights reserved by her from various sources have been duly acknowledged. No part of this thesis has been submitted elsewhere for award of any other degree.

Date: 21-11-2023

Place: Tezpur University

(Prof. Swapan Kumar Deka)

Supervisor



तेजपुर विश्वविद्यालय / TEZPUR UNIVERSITY
(संसद के अधिनियम द्वारा स्थापित केंद्रीय विश्वविद्यालय)
(A Central University established by an Act of Parliament)

Swapan Kumar Dolui
Professor
Department of Chemical Sciences

Mobile: +91-9957198489
Email: dolui@tezu.ernet.in

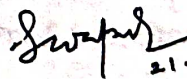
CERTIFICATE FROM SUPERVISOR

This is to certify that the thesis entitled "*Development of Electrocatalysts for Hydrogen Evolution Reaction in Acidic Medium*" submitted to the School of Sciences, Tezpur University in partial fulfillment for the award of the degree of Doctor of Philosophy in Chemical Sciences is a record of research work carried out by **Ms. Suman Lahkar** under my supervision and guidance. She has been duly registered (Registration No. TZ156024 of 2015), and the thesis presented is worthy of being considered for Ph.D. Degree.

All help received by her from various sources have been duly acknowledged. No part of this thesis has been submitted elsewhere for award of any other degree.

Date: 21-11-2023

Place: Tezpur University


21.11.23

(Prof. Swapan Kumar Dolui)

Supervisor



तेजपुर विश्वविद्यालय / TEZPUR UNIVERSITY
(संसद के अधिनियम द्वारा स्थापित केंद्रीय विश्वविद्यालय)
(A Central University established by an Act of Parliament)

Panchanan Puzari
Professor
Department of Chemical Sciences

Mobile: 91-8486872235
Phone: 0-3712-275061
Email: pancha@tezu.ernet.in

CERTIFICATE FROM CO-SUPERVISOR

This is to certify that the thesis entitled entitled "*Development of Electrocatalysts for Hydrogen Evolution Reaction in Acidic Medium*" submitted to the School of Sciences, Tezpur University in partial fulfillment for the award of the degree of Doctor of Philosophy in Chemical Sciences is a record of research work carried out by **Ms. Suman Lahkar** under my supervision and guidance. She has been duly registered (Registration No. TZ156024 of 2015), and the thesis presented is worthy of being considered for Ph.D. Degree.

All help received by her from various sources have been duly acknowledged. No part of this thesis has been submitted elsewhere for award of any other degree.

Date: 21-11-2023

Place: Tezpur University

(Prof. Panchanan Puzari)

Co-Supervisor

ACKNOWLEDGEMENT

This journey has remained a challenging one for me in many ways. I would not have been able to accomplish this path without continuous support, encouragement, faith, and blessings from numerous individuals. It is a pleasant honor to convey my heartiest thanks to all who offered help and support during this journey.

I would like to pay my respect and deepest gratitude to my esteemed supervisor Prof. Swapan Kumar Dolui for his valuable suggestions, inspiring guidance, fatherly care and encouragement throughout my research tenure. Above all his helpful nature, his positive and encouraging attitude immensely helped me to stay positive during my hard time. Thank you, Sir, for all you have done for me. I will be indebted to you forever in my life.

I will be forever grateful to my Co-supervisor Prof. Panchanan Puzari for his support, guidance, and encouragement throughout my PhD tenure. Thank you, Sir, for your support whenever I need.

I remain thankful to my doctoral committee member, Prof. Robin Kumar Dutta for his support and suggestions. I take this opportunity to thank the Department of Chemical Sciences and Head of the Department of Chemical Sciences, for providing access to all the available departmental facilities in my research work. Also, I would like to thank all the faculty members of the Department of Chemical Sciences for their valuable suggestions.

My sincere gratitude goes to the Vice-Chancellor, Tezpur University for providing us a good environment to live in and all the research facilities for the completion of my research work.

My special appreciations go to all the technical staff of the Department of Chemical Sciences and SAIC, Tezpur University for their constant help and support during my research work.

I would like to extend my warm thanks to all my dearest friends for their inspiration, support and valuable suggestions. I really want to thank my past lab members Dr. Kiranjyoti Mohan, Dr. Anindita Bora, Dr. Junali Handique, Dr. Jayashree Nath, Dr. Simanta Doley, Dr. Priyankamoni Saikia, my present lab members Shahnaz, Asfi, Parveen, and Kankana for their help in my research, their love and emotional support. I really appreciate all the great times we have spent together which makes my PhD journey quite beautiful and memorable. My warm

thanks to Mr. Nayab Hussain, Ms. Dimpi Sarmah and Ms. Kashmiri Boruah for their support throughout my PhD tenure.

My most loving gratitude sincerely goes to my parents for their countless sacrifice, for being my backbone whenever I fall back, their constant prayers and encouragement to become better version of myself. Thank you, Ma Deta, for all your sacrifice and support, I really think words simply don't express all that I feel and respect for you. Last but certainly not the least, I would like to thank the Almighty God for always there whenever I need help, to correct my path whenever I got distracted. Thank you for your blessings.

November, 2023

Tezpur University

Suman Lahkar

ABBREVIATIONS AND SYMBOLS USED

Ag/AgCl	silver/silver chloride
As	arsenic
A	area
APS	ammonium persulfate
A g ⁻¹	Ampere per gram
B	boron
BET	Brunauer-Emmett-Teller
BJH	Barrett–Joyner–Halenda
CO ₂	Carbon dioxide
CO	carbon monoxide
CB	conduction band
CoS	cobalt sulphide
CoS ₂	cobalt disulphide
Co	cobalt
Cu	copper
Cd	cadmium
CoP	cobalt phosphide
C	carbon
CV	cyclic voltammetry
C	capacitance
CA	chronoamperometry
C ₁	resistance between two parallel circuits composed of resistors and constant phase elements
CPE	constant phase elements
<i>C_{dl}</i>	electrochemical double-layer capacitance (<i>C_{dl}</i>)
<i>C_{sc}</i>	capacitance of the space charge layer
COOH	carboxylic acid
CH ₃ OH	methanol
C ₆ H ₅ NH ₂	aniline
CH ₃ COOH	acetic acid
D	dimensional
DFT	density functional theory

eV	electron volt
e ⁻	electron
ECSA	electrochemical surface area
EDLC	electric double-layer capacitor
EG	expanded graphite
EDX	elemental dispersive X-ray spectrometry
EIS	electrochemical impedance spectroscopy
$\Delta E(H^*)$	energy change of hydrogen adsorption
E_{fb}	flat band potential
FeS	iron sulphide
F	Faraday constant
FTIR	Fourier transform infrared spectroscopy
FESEM	field emission scanning electron microscopy
Fe(NO ₃) ₃ ·9H ₂ O	iron (III) nitrate nonahydrate
GCE	glassy carbon electrode
$\Delta G_{H_{ads}}$	free energy of adsorbed hydrogen
GCD	galvanostatic charge-discharge
HER	hydrogen evolution reaction
H ⁺	proton
H ₂ O	water
H ₂	hydrogen
h	hour
H _{ads}	adsorbed hydrogen
H ₂ SO ₄	sulphuric acid
HDS	hydrodesulphurization
Hz	hertz
H ₂ PtCl ₆	chloroplatinic acid
H ₂ O ₂	hydrogen peroxide
HCHO	formaldehyde
IEA	International Energy Agency
IRENA	International Renewable Energy Agency
i ₀	exchange current density
Ir	iridium
i	current

j	current density
J	current density
J_0	exchange current density
J-V plot	current-voltage plot
KOH	potassium hydroxide
kHz	kilohertz
KSCN	potassium thiocyanate
KMnO ₄	potassium permanganate
kW kg ⁻¹	kilowatt per kilogram
LSV	linear sweep voltammetry
Li	lithium
Mt	megatonne
M	active metal site
MoS ₂	molybdenum disulphide
Mo	molybdenum
MoSe ₂	molybdenum selenide
mA cm ⁻²	milliampere per centimeter square
mV	millivolt
Mo ₂ C	molybdenum carbide
MOF	metal-organic framework
MoB ₂	molybdenum boride
MWCNT	multi-walled carbon nanotube
Mo ₂ N	molybdenum nitride
mV dec ⁻¹	millivolt per decade
MnO ₂	manganese dioxide
mHz	millihertz
mV sec ⁻¹	millivolt per second
M-S	Mott-Schottky
mM	millimole
M	molar
NADPH	nicotinamide adenine dinucleotide phosphate hydrogen
nm	nanometer
NHE	normal hydrogen electrode
NiS ₂	nickel disulphide

Ni	nickel
Ni ₅ P ₄	penta nickel phosphide
Ni ₃ S ₂	tri nickel disulphide
NiP	nickel phosphide
N	nitrogen
n	number of electrons transferred
Na ₂ SO ₄	sodium sulphate
<i>N_D</i>	charge carrier density
NaDDBS	sodium dodecylbenzenesulfonate
NaBH ₄	sodium borohydride
NaOH	sodium hydroxide
NaNO ₃	sodium nitrate
Na ₃ PO ₄	sodium hypophosphate
Na ₂ CO ₃	sodium carbonate
Na ₃ PO ₄ ·12H ₂ O	sodium phosphate dodecahydrate
(NH ₄) ₂ S ₂ O ₈	ammonium peroxodisulfate
OER	oxygen evolution reaction
O ₂	oxygen
P	phosphorous
Pt	platinum
P	power density
PANI	polyaniline
PPY	polypyrrole
PDOS	Projected density of states
q	charge
Q	charge
RDS	rate-determining step
Ru	ruthenium
RGO	reduced graphene oxide
R	resistance
RHE	reversible hydrogen electrode
<i>R_{ct}</i>	charge-transfer resistance
R ₂	charge transfer resistance
R ₁	solution resistance arising from the electrolyte

R_f	roughness factor
rpm	rotation per minute
S	sulphur
SWCNT	single-walled carbon nanotube
SEM	scanning electron microscopy
ΔS	entropy change of adsorption H
SCE	standard calomel electrode
SCN ⁻	thiocyanate ion
Se	selenium
sec	second
TOF	turn over frequency
TMSes	transition metal selenides
TMSs	transition metal selenides
Ti	titanium
TiO ₂	titanium dioxide
Ti ₂ O ₃	titanium (III) dioxide
TMD	transition metal dichalcogenide
T	temperature in kelvin
TOF	Turn Over Frequency
TEM	transmission electron microscopy
TMPs	transition metal phosphides
TOP	trioctylphosphine
TiOOH	titanium (oxy)hydroxides
TTIP	titanium tetraisopropoxide
TEABF ₄	tetraethyl ammonium tetrafluoroborate
UV	ultraviolet
V	volt
VB	valence band
V _{hexane}	volume of hexane
V _{ethanol}	volume of ethanol
W	tungsten
W h kg ⁻¹	watt hour per kg
XRD	X-ray diffraction
XPS	X-ray photoelectron spectroscopy

Zn	zinc
ΔZPE	zero-point energy change
γ	gamma
η	overpotential
α	symmetry factor
ϵ_0	permittivity of free space
ϵ_r	relative permittivity of the dielectric medium
λ	wavelength
θ	angle between the individual atomic planes
α_c	charge transfer coefficient for the cathodic potential
Ω	ohm
ν	scanning rate
μF	microfarad
$^{\circ}C$	degree Celsius

LIST OF FIGURES

		Page No.
Chapter 1: General introduction		
Figure 1.1	Energy resources for worldwide energy consumption according to the data of 2023 Statistical Review of World Energy.	1.1
Figure 1.2	Advantages of hydrogen as a fuel obtained from water splitting.	1.2
Figure 1.3	Different sources used for hydrogen production according to International Renewable Energy Agency (IRENA) 2021.	1.3
Figure 1.4	Schematic representation of the photocatalytic water splitting reaction.	1.5
Figure 1.5	Schematic representation of photoelectrocatalytic water splitting reaction.	1.6
Figure 1.6	Band energy states of various semiconductors.	1.7
Figure 1.7	Three-electrode cell compartment used in the laboratory to study electrocatalytic HER.	1.7
Figure 1.8	HER mechanisms and various steps involved in each of them.	1.9
Figure 1.9	Relationship between i_0 and ΔG on HER volcano plot.	1.10
Figure 1.10	Different polymorphs of titanium oxide.	1.14
Figure 1.11	Various surface morphologies of the catalysts for HER to improve the reaction efficiency.	1.15
Figure 1.12	Different forms of carbon and its favorable properties for use in catalytic applications.	1.17
Figure 1.13	Performance comparison of supercapacitors and batteries on Ragone plot.	1.21
Figure 1.14	Schematic representation of the performance principle of EDLC.	1.23
 Chapter 2: Modulation of electronic density states of carbon in Expanded Graphite via multifaceted Cu doped Co₂P particle for electrocatalytic hydrogen evolution reaction in aqueous acidic medium		
Figure 2.1	XRD patterns of (a) natural graphite flakes and EG, (b) EG, Cu _{0.005} Co ₂ P and Cu _{0.005} Co ₂ P@EG, (c) Co ₂ P, Cu _{0.003} Co ₂ P, Cu _{0.005} Co ₂ P and Cu _{0.01} Co ₂ P (right part is the magnified image for the significant (111) plane of the respective composites).	2.7
Figure 2.2	FTIR spectra of EG and Cu _{0.005} Co ₂ P@EG.	2.9
Figure 2.3	SEM images of (a) graphite, (b, c) EG and (d) Cu _{0.005} Co ₂ P@EG; (e, f) TEM images showing hollow Cu doped Co ₂ P particles reside in the hive structure of EG at different resolutions; (g, h) HRTEM images of the composite with significant (111) plane of Co ₂ P particles and (002) plane corresponding to EG.	2.10
Figure 2.4	(a) EDX spectra of Cu _{0.005} Co ₂ P@EG and elemental distribution of (b) C, (c) Cu, (d) Co and (e) P.	2.11
Figure 2.5	High-resolution XPS spectra of (a) C 1s, (b) Co 2p, (c) Cu 2p and (d) P	2.11

2p of $\text{Cu}_{0.005}\text{Co}_2\text{P@EG}$ respectively.

Figure 2.6	Electrocatalytic performances of the catalysts in 0.5 M H_2SO_4 in terms of (a,c) their polarization curves and (c, d) Tafel plots.	2.13
Figure 2.7	Nyquist impedance plots of various catalysts.	2.16
Figure 2.8	(a) Cyclic voltammograms at various scan rate from 20 mV s^{-1} to 220 mV s^{-1} within a non-faradic region for (a) Co_2P , (b) $\text{Cu}_{0.005}\text{Co}_2\text{P}$, and (c) $\text{Cu}_{0.005}\text{Co}_2\text{P/EG}$, (d) Variation of double layer charging current density against scan rate of the synthesized catalysts.	2.17
Figure 2.9	a) M-S plots measured at 0.1 kHz, (b) electrochemical stability of Cu doped $\text{Co}_2\text{P/EG}$ measured from CV profiles recorded at 50 mV s^{-1} up to 1000 cycles and (c) time dependence study at an overpotential of 8 mV in 0.5 M H_2SO_4 .	2.18
Figure 2.10	HER performances for catalyst (a) $\text{Cu}_{0.005}\text{Co}_2\text{P@EG}$ and (b) $\text{Cu}_{0.005}\text{Co}_2\text{P}$ with and without the addition of KSCN in the electrolyte.	2.20
Figure 2.11	Minimum energy structures of (a) EG, (b) $\text{Co}_2\text{P@EG}$ and (c) Cu doped $\text{Co}_2\text{P@EG}$.	2.21
Figure 2.12	Comparison of projected density of states (DOS) of H(1s) and its bonded C(2p) when H is adsorbed on the surface of pristine EG, $\text{Co}_2\text{P@EG}$, and Cu doped $\text{Co}_2\text{P@EG}$. The dashed lines represent the centre of the occupied band.	2.22

Chapter 3: Iron doped titania/multiwalled carbon nanotube nanocomposite: a robust electrocatalyst for hydrogen evolution reaction in aqueous acidic medium

Figure 3.1	XRD patterns of (a) TiO_2 and acid functionalized MWCNT, (b) Fe doped $\text{TiO}_2/\text{MWCNT}$ and Fe doped TiO_2 .	3.6
Figure 3.2	FTIR spectra of MWCNT, Fe doped TiO_2 and Fe doped $\text{TiO}_2/\text{MWCNT}$.	3.7
Figure 3.3	SEM images showing surfaces of (a) MWCNT, (b) acid functionalized MWCNT(c,d) Fe doped $\text{TiO}_2/\text{MWCNT}$, (e) EDX spectra; (f,g) TEM image showing surface of the composite, the inset of (g) shows a cracked portion of the composite that leads the MWCNT pull out; (h) HRTEM image showing accumulation of metal particles on MWCNT backbone alongwith (002) plane of MWCNT (The inset focused HRTEM shows (101) plane of anatase) and (i) SAED pattern of Fe doped $\text{TiO}_2/\text{MWCNT}$.	3.8
Figure 3.4	Electrocatalytic performances of Pt wire, Fe doped $\text{TiO}_2/\text{MWCNT}$, platinumized Fe doped TiO_2 , Fe doped TiO_2 and bare TiO_2 in terms of their (a) polarization curves and (b) Tafel Plots; Performances of Fe doped $\text{TiO}_2/\text{MWCNT}$ with varying MWCNT content (wt%=0.65, 0.50, 0.35) in terms of their (c) polarization curves and (d) Tafel plots.	3.10

Figure 3.5	Cyclic voltammograms at various scan rate within a non-faradic region for (a) Fe doped TiO ₂ and (b) Fe doped TiO ₂ /MWCNT, (c) charging current density against scan rate (C_{dl} values calculated for Fe doped TiO ₂ and Fe doped TiO ₂ /MWCNT).	3.12
Figure 3.6	Nyquist impedance plots of various catalysts.	3.13
Figure 3.7	Electrochemical stability of Fe doped TiO ₂ /MWCNT: (a) CV profiles recorded at 20 mV s ⁻¹ up to 1000 cycles and (b) time dependence study at a static overpotential of 217 mV in 0.5 M H ₂ SO ₄ .	3.14

Chapter 4: Iron doped titania/ Polyaniline composite: an efficient electrocatalyst for hydrogen evolution reaction in acidic medium

Figure 4.1	XRD pattern of (a) Comparison of Fe doped TiO ₂ and TiO ₂ , (b) Fe doped TiO ₂ @PANI, Fe doped TiO ₂ and PANI.	4.4
Figure 4.2	FTIR spectra of pure PANI and Fe doped TiO ₂ @PANI.	4.5
Figure 4.3	SEM images of (a) pure PANI, (b) Fe doped TiO ₂ @PANI, (c) EDX spectra of Fe doped TiO ₂ @PANI, (d, e) TEM images of Fe doped TiO ₂ @PANI at various resolutions shows distribution of Fe doped TiO ₂ nanoparticles on PANI and (f) HRTEM of Fe doped TiO ₂ @PANI with lattice fringes corresponding to d (101) plane and d (200) planes.	4.6
Figure 4.4	High-resolution XPS spectra of Fe doped TiO ₂ @PANI (a) C 1s, (b) N 1s, (c) Ti 2p, (d) O 1s and (e) Fe 2p.	4.7
Figure 4.5	Electrocatalytic performance of various catalysts (a) Polarization curves showing onset potentials for HER (b) Tafel plots.	4.8
Figure 4.6	Nyquist plots of various synthesized materials.	4.10
Figure 4.7	Time dependence study of the catalyst Fe doped TiO ₂ @PANI at an overpotential of -200 mV (Vs RHE) in 0.5 M H ₂ SO ₄ .	4.11
Figure 4.8	(a) cyclic voltammograms at various scan rates from 20 mV s ⁻¹ to 220 mV s ⁻¹ within a non-faradic region, (b) variation of double layer charging current density against scan rate (C_{dl} values calculated for PANI and Fe doped TiO ₂ @PANI).	4.12

Chapter 5: Bi-functional hierarchically porous N, P co-doped reduced graphene oxide aerogel as a symmetric supercapacitor material and a robust hydrogen evolution reaction electrocatalyst

Figure 5.1	XRD patterns of N, P doped RGO aerogel i) before pyrolysis, pyrolysis at ii) 800 ⁰ C and at iii) 900 ⁰ C.	5.5
Figure 5.2	BET isotherms of (a) N doped RGO aerogel and (b) N, P co-doped RGO aerogel and the inset shows the corresponding pore size distribution curves.	5.6

Figure 5.3	RAMAN spectra of N doped RGO aerogel 800 and N, P doped RGO aerogel 800.	5.8
Figure 5.4	High resolution XPS spectra of N, P doped RGO aerogel 800.	5.9
Figure 5.5	Morphological studies of N, P doped RGO aerogel (a-c) SEM images at different magnification, EDX spectra of N, P doped RGO aerogel at different temperature (d) 600 ⁰ C, (e) 800 ⁰ C and (f) 1000 ⁰ C.	5.10
Figure 5.6	TEM images of N, P doped graphitic carbon at low resolution (a-b) and at high resolution (c) showing the presence of a large number of mesopores, (d) SAED pattern represents the planes corresponding to (100) and (002) plane.	5.11
Figure 5.7	CV curves of the different electrode materials in a three-electrode configuration at a scan rate of 50 mV sec ⁻¹ , (b) the CV curves of N, P co-doped RGO aerogel at different scan rates, (c) charge-discharge tests of the synthesized materials at a current density of 10 A g ⁻¹ , and (d) electrochemical impedance spectra of N doped RGO aerogel and N, P co-doped RGO aerogel electrodes in a three-electrode cell fitted with an equivalent circuit as shown in the inset of (d).	5.12
Figure 5.8	CV at different potential windows from (-0.2 V to 1.2 V) to (-0.8 V to 1.2 V) at a scan rate of 50 mV sec ⁻¹ , (b) CV at different scan rates (from inner to outer: 10, 25, 50, 70 and 100 mV s ⁻¹).	5.15
Figure 5.9	(a) charge-discharge tests at different current densities: 1, 5, 10 A g ⁻¹ , (b) charge-discharge tests at higher current densities: 15, 20, 25, 30 and 35 A g ⁻¹ , (c) variation of calculated C _{sp} with current density.	5.16
Figure 5.10	Performance of the device during 2000 cycles of the catalyst N, P doped RGO aerogel in two electrode cell measurements.	5.17
Figure 5.11	Ragone plot of N, P co-doped RGO aerogel as symmetric supercapacitor for its performance comparison with other carbon-based supercapacitors.	5.17
Figure 5.12	Figure 5.12 (a) GCD curves of the supercapacitor at different operating temperatures from 40 ⁰ C to 60 ⁰ C at a current density of 5 A g ⁻¹ , b) EIS at different working temperatures and (c) variation of R _{CT} of the supercapacitor with temperature.	5.19
Figure 5.13	Electrocatalytic performances of the catalysts in 0.5 M H ₂ SO ₄ in terms of their a) polarization curves and b) Tafel plots.	5.20
Figure 5.14	a) electrochemical stability of N, P co-doped RGO aerogel as measured from CV profiles recorded at 50 mV s ⁻¹ upto 1000 cycles and b) time dependence study at an overpotential of 100 mV in 0.5 M H ₂ SO ₄ .	5.22

EXPERIMENTAL SCHEME

Chapter 2: Modulation of electronic density states of carbon in Expanded Graphite via multifaceted Cu doped Co₂P particle for electrocatalytic hydrogen evolution reaction in aqueous acidic medium Page No.

Scheme 2.1 Experimental scheme of synthesis of Cu doped Co₂P@EG composites and the drop casting process.

LIST OF TABLES

Chapter 2: Modulation of electronic density states of carbon in Expanded Graphite via multifaceted Cu doped Co₂P particle for electrocatalytic hydrogen evolution reaction in aqueous acidic medium Page No.

Table 2.1 Double layer capacitance C_{dl} , roughness factor R_f and electrochemical active surface area ECSA values obtained for different catalysts. 2.18

Table 2.2 Donor density N_D and flat band potential E_{fb} values obtained for different catalysts. 2.19

Table 2.3 Adsorption free energy ($\Delta G(H^*)$) for various models (in eV). 2.23

Table 2.4 Comparison of activities of different cobalt phosphide-based catalysts towards HER. 2.23

Chapter 3: Iron doped titania/multiwalled carbon nanotube nanocomposite: a robust electrocatalyst for hydrogen evolution reaction in aqueous acidic medium

Table 3.1 Double layer capacitance C_{dl} , roughness factor R_f and electrochemical active surface area ECSA values obtained for different catalysts. 3.13

Table 3.2 Comparison of activities of different TiO₂ and CNT based catalysts towards HER. 3.15

Chapter 4: Iron doped titania/ Polyaniline composite: an efficient electrocatalyst for hydrogen evolution reaction in acidic medium

Table 4.1 C_{dl} , R_f and ECSA values obtained for PANI and Fe doped TiO₂/PANI. 4.12

Chapter 5: Bi-functional hierarchically porous N, P co-doped reduced graphene oxide aerogel as a symmetric supercapacitor material and a robust hydrogen evolution reaction electrocatalyst

Table 5.1 Comparison of the performances of different carbon-based symmetric supercapacitors. 5.18